esteem3

Enabling Science through European Electron Microscopy

Third Report on TEM methods applied to ICT material

Deliverable D7.3 – version 5

Estimated delivery date:	December 2022
Actual delivery date:	January 2023
Lead beneficiary:	CNRS
Person responsible:	Alexandre Gloter, Raul Arenal, Gerald Kothleitner
Deliverable type:	☒ R ☐ DEM ☐ DEC ☐ OTHER ☐ ETHICS ☐ ORDP
Dissemination level:	PUBLIC

THIS PROJECT HAS RECEIVED FUNDING FROM THE EUROPEAN UNION'S HORIZON 2020 RESEARCH AND INNOVATION PROGRAMME UNDER GRANT AGREEMENT NO **823717**

Grant Agreement No:	823802
Funding Instrument:	Research and Innovation Actions (RIA)
Funded under:	H2020-INFRAIA-2018-1: Integrating Activities for Advanced Communities
Starting date:	01.01.2019
Duration:	54 months

Revision history log

Version number	Date of release	Author	Summary of changes
V1	01/01/2023	Alexandre Gloter (CNRS-ORS)	First draft of the deliverable
V2	02/01/2023	Raul Arenal	Minor corrections - Finalization
V3	03/01/2023	Gerald Kothleitner	Minor corrections
V4	04/01/2023	Peter A. van Aken	Approval
V5	09/01/2023	Lucie Guilloteau	Editing

Table of contents

Introduction

The ICT industry's use of electronic, magnetic, photonic and semiconducting materials is vital to guarantee the quality and usability of future generations of Information and Communications Technologies. To gain an understanding of these materials in order to exploit them effectively, powerful characterization techniques such as diffraction and imaging, electron tomography, spectroscopy, holography and *in situ* studies are needed. This work package investigates the applicability of transmission electron microscopy (TEM) for this purpose by splitting its activities into three tasks; however due to their interrelated nature some results may overlap between tasks. This deliverable will focus on the major discoveries made in the last two-year time span of this project.

Task 7.1: Semiconducting and magnetic materials (GRA, ZAR, CHA, TOU*, CAT*)

Semiconducting and magnetic materials are essential for the development of modern Information and Communications Technologies (ICT). Advances in these technologies, such as miniaturization, scalability, storage density have been largely enhanced by semiconductor devices. In recent years, there has also been an interest in magnetic materials for ICT applications – not only for data storage media but also due to their potential properties that can be used to facilitate faster computing speeds as well as low power consumption. Thus, semiconducting and magnetic materials have become a highly sought-after technology providing many tremendous advances advantageous both now and in future. It has motivated many TEM related experiments for semiconducting and magnetic materials during this project.

Several magnetic materials have been investigated, such as spinodally decomposed alloys, notably via the use of DPC techniques (GRA, [Radlinger et al. 2022]) or the complex structure of iron oxide core-shell nanoparticles (ZAR, see detail below, figure 1 [Sartori et al. 2021]). Semiconducting materials have also been thoroughly investigated, with several examples from CHA: An in-situ mechanical and electrical TEM study on NW was conducted with the goal of tuning hole mobility of individual p-GaAs nanowires using uniaxial tensile stress (CHA, see detail below, figure 2 [Zeng et al. 2021]). Uniaxial strain has also been used to tune photocurrent in single GaAs p–i–n junctions (CHA, [Holmer 2021]), and epitaxial Pb on InAs nanowires for quantum devices was reported [Kanne et al. 2021] (CHA).

Nanoparticles combining several magnetic phases offer potential applications such as data storage or sensors due to their high modularity. Sartori et al. [2021] reports on the synthesis of $Fe_{3-\delta}O4@CoFe_2O_4@Fe_{3-\delta}O_4$ onion-like nanoparticles through a three-step seed-mediated growth approach at 300 °C. TEM, EELS, Mössbauer spectrometry, XAS and XMCD reveal changes in chemical composition and core/shell thicknesses, which greatly impact magnetic properties. This highlights the great potential of onion-like nanoparticles to tune magnetic characteristics for various desired applications. It is for instance reported that CS (core-shell) and CSS (core-shell-shell) nanoparticles display enhanced magnetic anisotropy energies in comparison to C (core) nanoparticles as a result of strong exchange coupling at the soft/hard and hard/ soft interfaces. Although the $Fe_{3-\delta}O_4$ shell is very thin and discontinuous, it has a significant influence on the magnetic properties of CSS nanoparticles. In comparison, pure $CoFe_2O_4$ nanoparticles with similar size to that of CSS display a similar value of TB (blocking temperature), although a much lower number of Co atoms were incorporated in the present case. Such a high control of the structure of the nanoparticles is particularly interesting to modulate their magnetic properties, thus extending their potential to a wide range of applications, but it requires quantitative STEM analysis, provided in this project (figure 1).

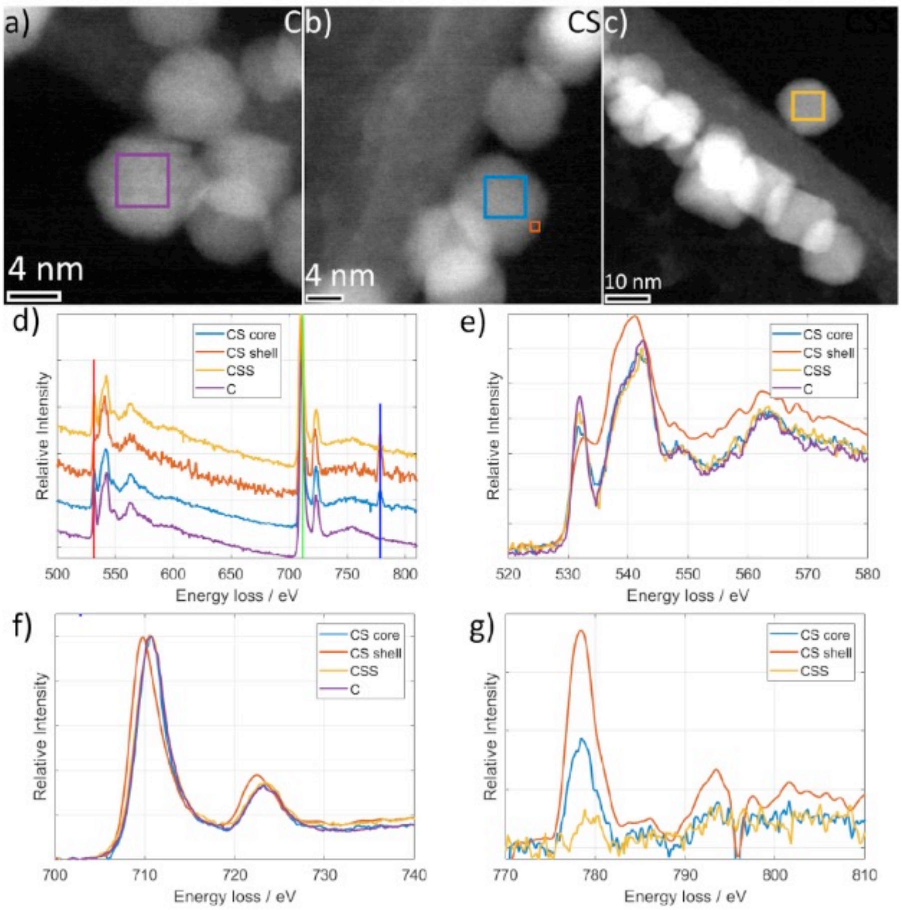

Figure 1: Dark-field images of (a) C, (b) CS, and (c) CSS nanoparticles. (d) Exemplary EELS spectra obtained from positions marked in (a–c) showing the O−K edge (532 eV, red vertical line), Fe−L (708 eV, green vertical line) edges as well as the Co−L edge (779 eV, blue vertical line) in cases of CS and CSS nanoparticles. The spectra are vertically displaced to improve visibility. (e–g) Comparison of the background-subtracted EELS spectra of the (e) O−K, (f) Fe−L, and (g) Co−L edges reveal fine structure changes induced by the presence of Co in comparison to the C spectra. The $Fe{-}L_3$ peak shifts to lower energies in case of high Co percentages (CS shell). All spectra are normalized to the $Fe{-}L_3$ peak. From [Sartori et al. 2021].

Strain engineering provides an effective way of tailoring the electronic and optoelectronic properties of semiconductor nanomaterials and nanodevices, giving rise to novel functionalities. Within this project, CHA presented direct experimental evidence of strain-induced modifications of hole mobility in individual gallium arsenide (GaAs) nanowires, using *in situ* transmission electron microscopy (TEM) [Kanne et al. 2021]. The conductivity of the nanowires varied with applied uniaxial tensile stress, showing an initial decrease of ∼5–20% up to a stress of 1–2 GPa, subsequently increasing up to the elastic limit of the nanowires. This is attributed to a hole mobility variation due to changes in the valence band structure caused by stress and strain. The corresponding lattice strain in the nanowires was quantified by *in situ* four-dimensional scanning TEM and showed a complex spatial distribution at all stress levels. Meanwhile, a significant red shift of the band gap induced by the stress and strain was unveiled by monochromated electron energy loss spectroscopy as shown in figure 2.

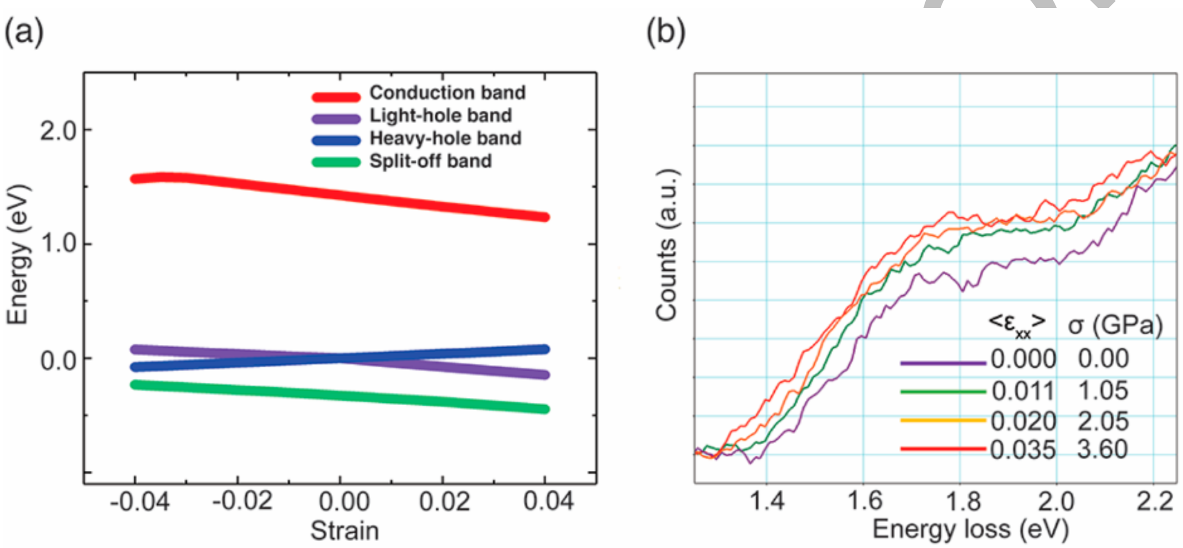

Figure 2: Effect of uniaxial stress and strain on the band structure of GaAs nanowires. (a) Tight binding simulation of band edges at the valence band top and conduction band bottom in GaAs and their shift as a function of strain along [111] direction. (b) *In situ* monochromated EELS spectra showing the red shift of the band gap onset of the GaAs nanowire under stress and strain. From [Kanne et al. 2021].

Task 7.2: Functional complex oxides, carbon and related nanostructures (ZAR, STU, ORS, TOU*)

Functional complex oxides are prime materials of choice for Information and Communications Technologies due to their unique physical, electronic, optical and magnetic properties, which enable novel technological applications. Furthermore, they offer possibilities for engineering multiple functionalities on a single substrate.

On that aspect, the interest of 2D gases in oxide thin films and at interfaces is attributed to their ability to exhibit strong electronic correlation effects and possible quantum fluctuations. These features have drawn considerable attention due to their potential for numerous intriguing physical phenomena such as metal-insulator transitions, high-temperature superconductivity, magnetoresistance or charge to spin current interconversion. Within this work-package, detection of 2D Electron Gas in TiO_2/LAO interface has been reported (GRA, article in preparation), the occurrence of a large and linear magnetoresistance in a $SrTiO_3$-based two-dimensional electron gas (ORS, [Mallik 2021], see Figure 3) and its origins have been elucidated thanks to STEM microscopy. Furthermore, the superfluid stiffness of a $KTaO_3$-based two-dimensional electron gas (ORS, [Mallik 2022]) have been discussed.

New developments for such oxide characterisation by TEM techniques or state of the art characterisation of new oxides materials have also been reported. We can cite, the online PACBED thickness determination (GRA, [Oberaigner 2023]), the quantitative atomic column loading and its quantitative determination on functional oxide within Ruddlesden-Popper phase (GRA, [Lammer 2022]), the determination of single Ta dopant atoms in STO (TUG, article in preparation) or the phase determination of $(Hf,Zr)O_4$ epitaxial films (ZAR, [Barriuso 2022]).

Such functional oxide materials are also characterized by the coupling of several orders that can control or engineer new properties. For instance, ferroelectricity (where charge and lattice orders couple to give birth to a ferroelectric displacement) has been addressed by the discovery of polar chirality in $BiFeO_3$ emerging from a peculiar domain wall sequence (ORS, [Fusil 2022]), or in the role of Ca Solubility in a $BiFeO_3$-based System (GRA [Haselmann 2022], see Figure 4). Ferroelectricity was also reported in 1D hollandite crystal by ZAR [Gomez 2021]. Manganite and nickelate, where lattice and charge coupling leads to metal-to insulator transitions, have also been investigated. Furthermore, we can cite the role of strain vs O vacancies in SMO films (ZAR [Langenberg et al. 2022]), the octahedra tilt suppression in nickelate thin films (ZAR, article in preparation), and the manipulation of a metal-to-insulator transition in manganite thin films (STU [Li 2022]). Finally, emerging multiferroism in EuTiO3 due to negative pressure and a corresponding spin and phonon orders coupling have been reported (STU [Zhao 2022]).

As mentioned above, occurrence of correlated 2D gas is pivotal in oxide interfaces and quantum materials. Indeed, quantum materials harbor a cornucopia of exotic transport phenomena challenging our understanding of condensed matter. Among these, a giant, non-saturating linear magnetoresistance (MR) has been reported in various systems, from Weyl semimetals to topological insulators. Its origin is often ascribed to unusual band structure effects, but it may also be caused by extrinsic sample disorder. During this project, it has been reported a very large linear MR in a $SrTiO_3$ two-dimensional electron gas and, by combining transport measurements with electron spectro-microscopy, show that it is caused by nanoscale inhomogeneities that are self-organized during sample growth (figure 3, [Mallik 2021]). It also reveals semiclassical Sondheimer oscillations arising from interferences between helicoidal electron trajectories, from which we determine the 2DEG thickness, in accordance with the EELS measurement. Our results bring insight into the origin of linear MR in quantum materials, expand the range of functionalities of oxide 2DEGs and suggest exciting routes to explore the interaction of linear MR with features like Rashba spin-orbit coupling.

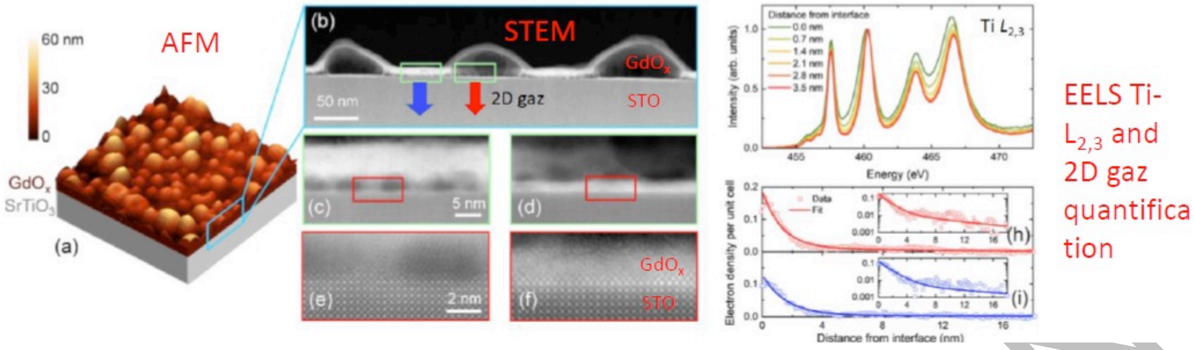

Figure 3: (a) AFM, (b) STEM, (C) EELS measured for the two family of 2D gases. 2D gases can occur at interfaces and exhibit properties absent in the bulk counterpart: for such GdOx/ SrTiO3interface, the 2D electrons gases exhibit a very large linear magnetoresistance (MR). The STEM-EELS (Ti-L) can now be done with atomic resolution and sub 100 meV resolution giving the possibility to measure quantitatively the electron occupations (Ti-3d) in these gases. Such spectro-microscopic work evidences that the large linear MR is caused by the mesoscopic structure (formation of blisters) and the electronic lateral inhomogeneities (Parish-Littlewood model for magnetotransport of inhomogeneous conductors), self-organized during the sample growth (adapted from [Mallik 2021]).

Ferroelectricity is a key element in ICT devices. It indeed allows non-volatile information storage. $BiFeO_3$ (BFO) is a prototypal ferroelectric whose structure has been optimized for decades. In BFO film, Bi_2O_3 (BO) is a known secondary phase, which can appear under certain growth conditions. However, BO is not just an unwanted parasitic phase, but can be used to create the super-tetragonal BFO phase in films on substrates, which would otherwise grow in the regular rhombohedral phase (R-phase). The super-tetragonal BFO phase has the advantage of a much larger ferroelectric polarization of 130–150 µC/cm^2, which is around 1.5 times the value of the rhombohedral phase with 80–100 µC/cm^2. During this project, it has been reported that the solubility of Ca, which is a common dopant of bismuth ferrite materials to tune their properties, is significantly lower in the secondary BO phase than in the observed R-phase BFO. Starting from the film growth, this leads to completely different Ca concentrations in the two phases as demonstrated by advanced analytical transmission electron microscopy techniques (Figure 4). The experimental results are further confirmed with density functional theory (DFT) calculations. At the film's fabrication temperature an about 50 times higher Ca concentration is expected in the BFO phase compared to the secondary one, caused by different solubilities. Depending on the cooling rate after fabrication, this can further increase, since a larger Ca concentration difference is expected at lower temperatures. This different Ca solubility between the two phases can prove problematic as it increases the Ca concentration in the BFO phase and could result in a critical change of its properties. This knowledge is essential when designing functional devices. Otherwise, an unexpected Ca concentration can potentially jeopardize the functionality of the BFO ferro-electric based device such as expected for non-volatile memory or neuromorphic computing.

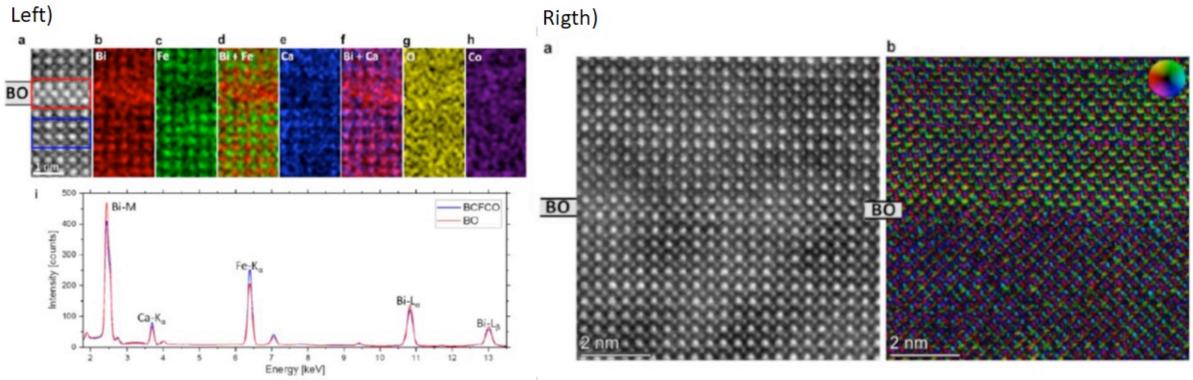

Figure 4: Left) EDS elemental analysis of a BO plate. (a) HAADF image of the EDS mapping area. The BO stripe is indicated on the left side. EDS elemental ratio maps of (b) Bi, (c) Fe, (d) Bi, and Fe combined, (e) Ca, (f) Bi and Ca combined, (g) O, and (h) Co. (i) Comparing the background-corrected and denoised spectra from the BO area of the red rectangle and the BCFCO area from the blue rectangle in (a). The spectra have the same colour as the associated rectangle. **Right)** DPC analysis of the ferroelectric polarization at a BO plate, which acts as a domain wall (a) HAADF STEM image of the BO plate and the area around it. The location of the BO plate is marked on the left and right side. (b) vector plot of the electric field retrieved from the DPC signal showing the two ferroelectric domains above and below the BO plate. Adapted from [Haselmann 2022].

Task 7.3: Photonic materials (GRA, ZAR, STU, ORS, CHA)

Recent research has sought to develop new plasmonic materials, as alternatives to traditional gold and silver. These new plasmonic materials might offer advantages in terms of cost and scalability over gold or silver. These materials can also be characterised by optical properties, which enable them to interact with light in a combined synergetic manner (e.g. combining plasmonic properties and photo-catalyst properties), enabling the potential for applications such as biosensing, solar energy harvesting, and boosted photo-catalyst efficacy. They can also represent a promising alternative for the use in telecommunication applications, if they exhibit a high quality factor in the NIR regime. Further study is needed into their suitability for use in these areas; however, they represent an exciting development in the field of plasmonics. A range of promising candidates have been identified within this project.

Among these alternatives, the project has reported the plasmonic properties for a correlated metal $SrVO_3$, from bulk to nanostructure demonstrating its high quality factor in the near infrared (ORS, [Su 2022]). We can also mention the case of Au/Rh plasmonic (GRA, article in preparation), with its potential for photocatalysis. The case of aluminium plasmonics on graphene has also been reported by uncovering the evolution of low-energy plasmons in nanopatterned aluminium plasmonics on graphene (STU, [Elibol 2022-1]) and by discussing the case of hybrid graphene-supported aluminium plasmonics (STU, [Elibol 2022-2]). For these latest examples, it has been demonstrated the adjustment of the charge-transfer-plasmon (CTP) resonances of aluminium (Al) bowties on suspended monolayer graphene via controlled nanofabrication and focused electron-beam irradiation. CTP resonances of bowties with a conductive junction blue-shift with an increase in junction width, whereas their 3λ/2 and λ resonances barely red-shift. These plasmon modes are derived and confirmed by an LC circuit model and electro-magnetic simulations performed with boundary-element and frequency-domain methods (Figure 5). A monotonic decay of the CTP lifetime is observed, while the junction width is ex-tended. Instead, the lifetimes of 3λ/2 and λ resonances are nearly independent of junction width. When the junction is shrunk by electron-beam irradiation, all antenna resonances red-shift. This work demonstrate the active control of CTP resonances and lifetime of Al plasmonics on the femtosecond time scale, which is crucial for applications, especially for ultrafast nano-switches.

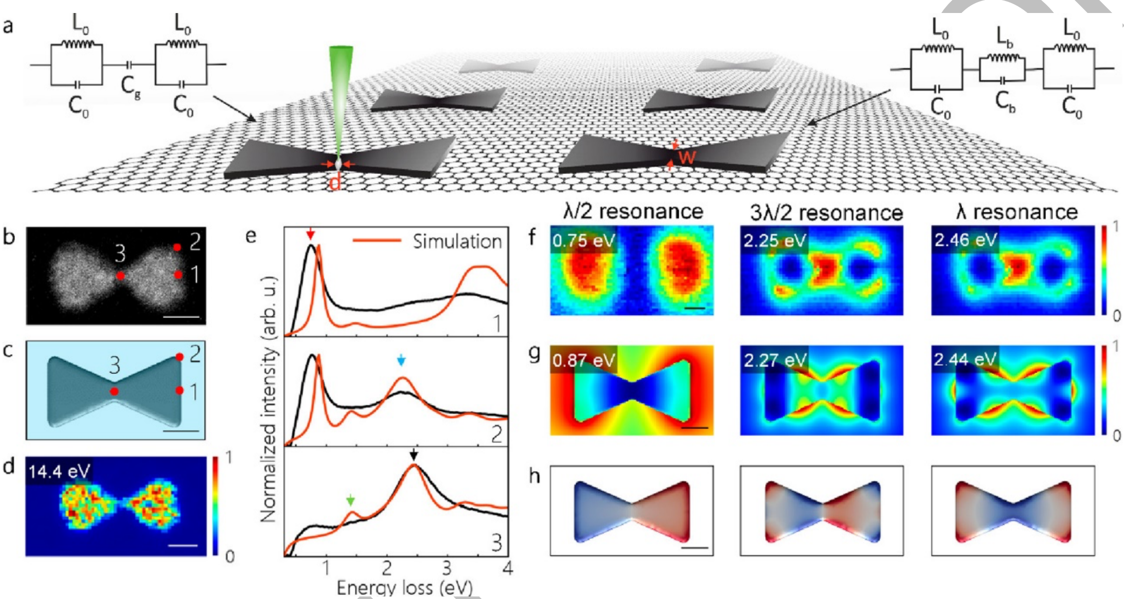

Figure 5: (a) Schematic of nanopatterned Al structures on suspended graphene and LC circuit models corresponding to the structures with and without a gap. Here, the gap is created by a focused electron beam. (b, c) HAADF image of a bowtie antenna with a conductive junction and its corresponding model used in BEM simulations, respectively. The effective medium surrounding the bowtie is shown in blue in (c). (d) Volume plasmon map for the bowtie in (b). (e) Experimental (black curves) and simulated (red curves) EEL spectra obtained at the positions marked with red dots in (b) and (c). The red, blue, and black arrows mark the λ/2 (CTP), 3λ/2, and λ resonances, while green arrows show the IBT. (f, g) Experimental and simulated EELS maps. (h) Computed eigenmodes corresponding to the CTP, 3λ/2, and λ resonances, respectively. The scale bars are 50 nm. From [Elibol 2022-1]

While alternative plasmonic materials have extensively been investigated, traditional plasmonic responses have also been studied for unusually geometries, such as ultra-high aspect ratio Au nanostructure (ZAR, [Pelaez-Fernandez 2022]). Within this work package, other studies have probed the optical properties for complex nano- or meso-structures such as the demonstration of whispering gallery mode selectivity through surface plasmons (ORS, [Auad 2022]) or for the second harmonic generation in germanium quantum wells for nonlinear silicon photonics (CHA, [Frigerio 2021]).

Summary

This project has provided insight into the capabilities of scanning transmission electron microscopy to study a diverse array of ICT materials. It has yielded extensive spectroscopic, structural and chemical information, while also allowing scientists to explore physical characteristics such as optical activity, transport and magneto-transport, optoelectricity, mangetism and mechanics. In conclusion, this project has effectively demonstrated the capability of STEM techniques in improving our understanding and allowing more informed advancement of these ICT materials.

References (selected papers only)

[Auad 2022] Auad et al., nanoletter 22 319 (2022)
[Barriuso 2022] *Nanomaterials 12*(7) (2022)
[Elibol 2022-1] Elibol and Van Aken, Nano Lett. 22(14):5825-5831 (2022)
[Elibol 2022-2] Elibol and Van Aken, ACS nano 16, 11931 (2022)
[Frigerio 2021] Frigerio et al., *ACS Photonics* 8, 3573 (2021)
[Fusil 2020] Fusil et al., Advanced ElectronicMaterials 8, 2101155(2022)
[Gomez 2021] Gomez et al. Nanoscale 9615 3 (2021)
[Haselmann 2022] Haselmann et al. J. Phys. Chem. C , 126, 7696–7703 (2022)
[Holmer 2021] Holmer et al., Nano Lett. , 21, 9038–9043(2021)
[Kanne 2021] Kanne et al., Nature Nanotechnology volume 16, pages 776–781 (2021)
[Lammer 2022] Lammer, Ultramicroscopy234 (2022) 113477
[Langenberg 2021] Langenberg et al. ACS omega 6 (20), 13144-13152 (2021)
[Li 2022] Li et al., phys Rev B 105, 165426 (2022)
[Mallik 2021] Mallik et al. 2021, Nano Letters 22, 65 (2021)
[Mallik 2022] Mallik et al. 2022, Nature Communications 13, 1-8 (2022)
[Oberaigner 2023], just accepted for publication in Microscopy and Microanalysis, Code availability: https://github.com/MichaelO1993/PACBED-CNN (2023)
[Pelaez-Fernandez 2022] Pelaez-Fernandez et al., Nanophotonics 11 3719 (2022)
[Radlinger 2022] Radlinger et al. J. Alloys Comp. 922 166214 (2022)
[Sartori 2021] Sartori et al. ACS Appl. Mater. Interfaces, 13, 14, 16784–16800 (2021)
[Su 2022]Su et al., Advanced optical materials 2202415 (2022)
[Zeng 2021] Zeng et al., Nano Lett., 21, 9, 3894–3900 (2021)
[Zhao 2022] Zhao et al. Nature com. 13, 2364 (2022)